Ultra-Stable Microwave Cryogenic Oscillator operated with a Gifford-McMahon cryocooler

G. Le Tetû[a], C. Fluhr[b], B. Dubois[b], J. Paris[c], R. Hostein[c], V. Giordano[a,*]

[a] *FEMTO-ST Institute, Time & Frequency Dpt., CNRS, 26 Chemin de l'Epitaphe, 25000 Besançon, France*
[b] *FEMTO Engineering, 32 Avenue de l'Observatoire 25000 Besançon, France*
[c] *PASQAL SAS, Cold and Vacuum Engineering Department, 7 Rue Léonard de Vinci, 91300 Massy, France*

Abstract

We demonstrate for the first time an ultra-stable microwave cryogenic oscillator operated with a Gifford-McMahon (GM) cryocooler. Despite the high level of vibration generated by the GM, we show that an optimised design, with simple passive solutions, enables a sufficient mechanical decoupling to achieve a state-of-the-art frequency stability. The implemented 10 GHz cryogenic oscillator features a fractional frequency stability (ADEV, Allan deviation) $\sigma_y(\tau) < 3\times10^{-15}$ for 1 s $\leq \tau \leq 10^4$ s.

Keywords: Pulse-Tube cryocooler, Gifford-McMahon cryocooler, Ultra-stable oscillator, Frequency stability.

1. Introduction

The cryogenic sapphire oscillator (CSO) is a highly specialised machine, which delivers a microwave reference signal exhibiting the lowest frequency fluctuations for measurement time up to 10^4 s[1, 2]. Thus, it shines in applications

*Corresponding author
Email address: giordano@femto-st.fr (V. Giordano)

[1]This work was supported by the LABEX Cluster of Excellence FIRST-TF (ANR-10-LABX-48-01), within the Program "Investissements d'Avenir" operated by the French National Research Agency (ANR). The authors would like to thank the Council of the Région de Franche-Comté for its support to the Program "Investissements d'Avenir".

where extremely low instability is critical and reliable unattended long-term operation is required. This is the case of the flywheel for primary frequency standards [3, 4], space navigation [5], radioastronomy or Very long Baseline Interferometry (VLBI) [6, 7], tests of fundamental physics [8, 9], or for quantum computing [10, 11].

The CSO is based on a sapphire mono-crystal resonating at 10 GHz in a whispering gallery mode [12], cooled at ≈ 6 K for zero thermal sensitivity and optimal quality factor. In our most advanced technology, codenamed ULISS-2G, the cryostat optimisation has enabled to operate the CSO with a low power Pulse-Tube (PT) cryocooler consuming only 3 kW (single phase) [13]. Thus, the CSO can be powered by a regular outlet (230 V 50 Hz, or 117 V, 60 Hz). ULISS-2G typically features a fractional frequency stability (ADEV, Allan deviation) $\sigma_y(\tau) < 3\times10^{-15}$, with $< 10^{-14}$ drift in one day [1]. This unprecedented performance is guaranteed with unattended operation between scheduled maintenance every two years. We already built and delivered seven ULISS-2G units to several National metrological Institutes and we are seeing growth in demand.

The PT technology has been chosen for its low level of mechanical vibrations. Indeed, the sapphire resonator being sensitive to the acceleration, the level of the mechanical vibrations limits the achievable frequency stability. ULISS-2G has been designed to maintain a sapphire temperature down to ~ 4 K with the 250 mW cooling power of the Cryomech PT403 cryocooler. It is the least powerful of the PT range of Cryomech citewww.cryomech. It operates with a 3 kW compressor and, to our knowledge, there is no equivalent product readily available on the market. For an obvious reasons of availability and to not hinder our future developments, we are actively looking for an alternative.

Oppositely, the Gifford-McMahon (GM) cryocooler is available from number of manufacturers with an extended range of cooling power. It is produced in larger quantities and generally cheaper. A secondary advantage of the GM is its

ability to operate in any orientation. This provides additional degrees of freedom in the cryostat design and could open the path for new applications. However, the main drawback of the GM cryocooler is its high level of vibrations compared to the PT. Nevertheless, the lessons learned and the many experiments gained over the past 10 years in building more than a dozen CSOs at the Femto-ST Institute have led us to the conclusion that a GM-based CSO is feasible. This paper summarises our design approach and the first tests carried out on such a prototype. It demonstrates that the GM cryocooler is an alternative solution to achieve an ultra-stable microwave oscillator.

2. The resonator acceleration sensitivity issue

Before to start the description of the cryogenic assembly, we need first to briefly focus on the acceleration sensitivity issue, which is recurring in the development of any ultra-stable oscillator. This issue was addressed in detail in the review article by Filler [15].

2.1. Theoretical framework

We recall here only the standard tools used to describe the degradation of the oscillator's performance due to its mechanical acceleration. Let's assume a resonator submitted to an acceleration a, its fractional frequency variation is:

$$\frac{\Delta\nu}{\nu_0} = \Gamma.a \tag{1}$$

ν_0 being the resonator unperturbed frequency, Γ its acceleration sensitivity, generally given in 1/g, with $g = 9.81$ m/s^2. In the general problem Γ and a are obviously both vector and the simple product in the equation 1 should be replaced by a scalar product. However, for simplicity, we will keep here the one dimensional description sufficient for our purposes. Let's assume that our resonator is submitted to a single tone periodic acceleration: $a(t) = \sqrt{2}\gamma \cos 2\pi f_m t$. Following the equation 1, the resonator frequency is modulated and for a small

perturbation a spurious line appears in the oscillator phase noise spectrum at the Fourier frequency f_m. The power contained in this line is given by:

$$S_\varphi(f_m) = \left(\frac{\Gamma\gamma\nu_0}{f_m}\right)^2 \tag{2}$$

expressed in rad^2, or more generally in dBrad^2.

In the time domain the fractional frequency stability is represented by the Allan Deviation (ADEV): $\sigma_y(\tau)$ as function of the integration time τ [16]. In the presence of the acceleration $a(t)$, the fractional frequency stability of the oscillator is degraded. The minimum achievable ADEV is given by:

$$\sigma_{y_{\min}}(\tau) = \left(\frac{\sqrt{2}\,\Gamma\gamma}{\pi\tau f_m}\right)\sin^2(\pi f_m \tau) \tag{3}$$

2.2. Specificities of the sapphire resonator

All the resonators we have integrated into our CSOs are manufactured according to the same design as shown in the figure 1.

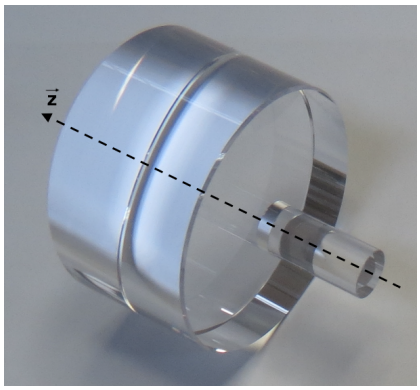

Figure 1: *The sapphire cryogenic resonator. The direction $O\vec{z}$ is conventionally aligned with the cylinder axis.*

The 10 GHz resonator is a cylinder, 54 mm in diameter and 30 mm in thickness, machined in a high quality sapphire (Al_2O_3) monocrystal. Placed in the centre of a copper cavity, it is cooled down near 6 K, where its thermal sensitivity vanishes at first order and its unloaded quality factor typically reaches

10^9. The 10 mm diameter spindle machined from the bulk is used to attach the resonator to the bottom flange of the copper cavity.

Currently, the sapphire resonator acceleration sensitivity is not accurately known. It arises from two physical effects:

- The *geometric* effect: Under the acceleration, the resonator shape changes, the mode frequency is thus shifted. At least in principle, this effect can be accurately calculated with current simulation multi-physic finite element softwares.
- the *dielectric* effect: the strain in the sapphire causes a change in its electrical permittivity. This effect is far more difficult to estimate. Indeed, the permittivity tensor sensitivity to a change in the state of the stress inside the sapphire is not known.

Theoretical estimations were proposed for the sensitivity along the cylindrical resonator axis ($O\vec{z}$): 2.4×10^{-9}/g [17] and 3.4×10^{-10}/g [18]. Some tests realised on a compact room temperature sapphire oscillator show that the acceleration sensitivity along the three axis is not higher than 5×10^{-10}/g [19]. In these last measurements, it is impossible to distinguish between the resonator sensitivity and those of the amplifier readout chain and of the control electronic circuits, which can partially compensate themselves.

2.3. Acceleration sensitivity measurements

Faced with this lack of precision on Γ, we have undertaken a new measurement based on the scheme depicted in the figure 2.

Here the sapphire resonator is operated at the room temperature. It is inserted in a cavity specially designed to repel any mechanical resonance above 1 kHz. It can be fastened on the platform of a mechanical shaker (TIRA VIB 2500 N) in two orthogonal directions. It is then possible to submit the resonator to an acceleration along its cylinder axis $O\vec{z}$ or in a transverse direction $O\vec{x}$. This mobile assembly includes also at the resonator input a microwave circulator and

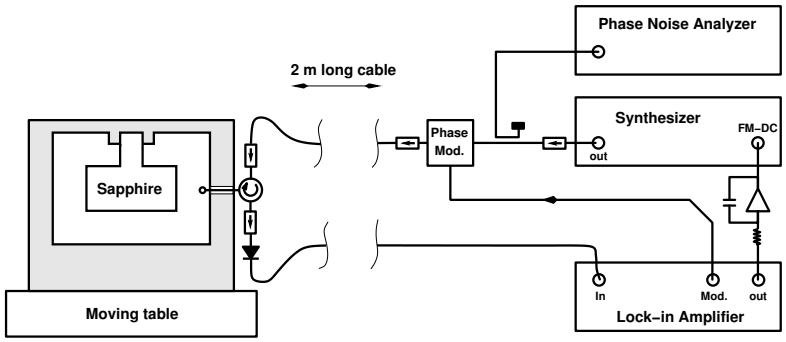

Figure 2: *Principle of the g-sensitivity measurement.*

a detection diode (D1), which are part of the frequency reference (see section 3.1). A microwave synthesiser is frequency locked on this reference by using a classical Pound servo loop [20, 21]. The synthesiser signal is phase modulated through an external voltage controlled phase shifter. The demodulation of the detection diode signal produces an error signal that after integration is sent to the synthesiser Frequency Modulation DC-input. The lock bandwidth is $\sim$ 30 kHz. The synthesiser signal is conveyed to the mobile frequency reference by a 2 m long flexible microwave cable (MiniCircuits CBL-2M-SMSM+). The latter is secured on rigid frames at different places to avoid mechanical resonances propagating along. The synthesiser phase noise is measured with the PM noise analyser Rohde & Schwarz FSWP26 [22]. When a single-tone acceleration at f_m is imposed by the shaker, a line at f_m appears in the phase noise spectrum. From the equation 2, we derive the resonator sensitivity Γ_u to an applied acceleration along the direction $O\vec{u}$ at the frequency f_m. The figure 3 shows the measurement results in the $O\vec{z}$ and $O\vec{x}$ directions as a function of the modulation frequency f_m. The dashed lines represent the detection limits, which have been determined by measuring independently the phase modulation inside the 2 m microwave cable when the shaker is moving.

We get for the 10 GHz sapphire resonator:

$$\Gamma_z = 1 \times 10^{-9}/\mathrm{g} \quad \text{and} \quad \Gamma_x = 3.1 \times 10^{-10}/\mathrm{g} \tag{4}$$

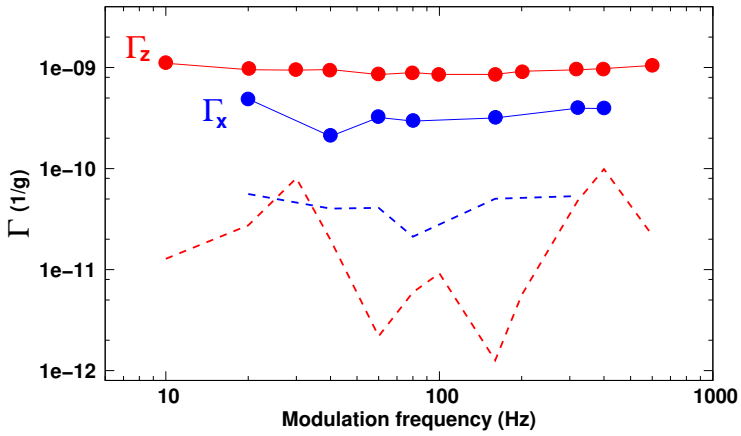

Figure 3: *Acceleration sensitivity of the sapphire resonator in the axial ($O\vec{z}$) and transverse ($O\vec{x}$) directions. The detection limits are represented by the dashed lines.*

We can now assess the maximum permissible acceleration. The figure 4 represents $\sigma_{y_{\min}}(\tau)$ for an acceleration along $O\vec{z}$ with $\gamma = 1$ and 10 μg. The resonator sensitivity is $\Gamma_z = 1 \times 10^{-9}$/g. The CSO frequency stability is ultimately limited at short-term by the noise floor of the Pound servo loop, which stabilizes the phase of the signal. For our CSO, this noise floor is typically of $7 \times 10^{-16}\tau^{-1/2}$ [23].

To ensure that a single-tone vibration at $f_m = 1$ Hz will not limit the frequency stability of the CSO above the ULISS-2G specification, i.e. $\sigma_y(\tau) \leq 3 \times 10^{-15}$ for $\tau > 1$ s, the maximum permissible rms acceleration in the axial direction is 10 μg (see Fig. 4). This corresponds to an rms axial displacement $z \sim 2.5$ μm.

3. Cryostat Design Overview

3.1. Cryogenic resonator assembly

The design of the ULISS-2G cryostat has been detailled in [13]. We keep here the same structure schematized in the figure 5.

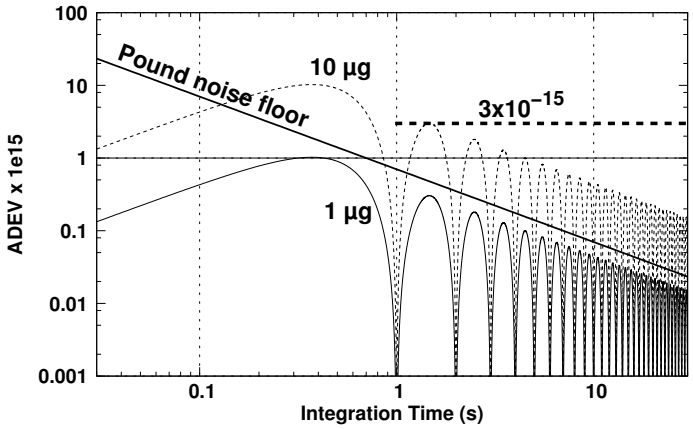

Figure 4: *ADEV limit of an oscillator with an acceleration sensitivity of* 1×10^{-9} *submitted to a rms acceleration of* $\gamma = 10$ μg *(dotted line) and* 1 μg *(plain line). Typical Pound noise floor (bold plain line). ULISS-2G spec (bold dashed line).*

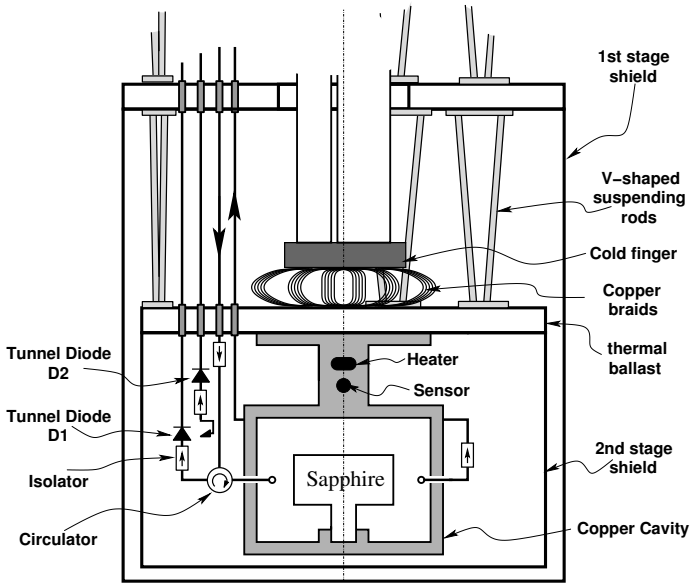

Figure 5: Sketch of the sapphire resonator mounting in the cryogenic environment.

The cavity is attached to the thermal ballast consisting of a 316L stainless steel (SS) plate 190 mm in diameter and 15 mm thick. A set of flexible OFHC copper braids thermally connects the ballast to the cryocooler 2^{nd}-stage. A

130 170 mm high gold-plated copper thermal shield is fastened to the ballast. The total mass to be cooled down to 6 K is approximately 7.5 kg. This assembly is suspended under the 1st-stage plate by a set of V-shaped rods to increase the stiffness in the transverse direction. In turn, the 1st-stage plate is suspended by similar rods under the top-flange of the cryostat vacuum chamber. The thermal
135 link to the cryocooler 1st-stage cold finger is realized with the another set of OFHC copper braids.

Four BeCu UT-085 2.2 mm diameter coaxial cables link the cryogenic assembly to the room temperature circuit. They are thermalised at each temperature
140 stage. Two of them are the resonator input and output ports and are connected to the sustaining amplifier placed at room temperature outside the cryostat. The other two convey the tunnel diode (D1 and D2) signals that are needed to stabilize the phase and the power of the signal injected in the cavity. Details on the sustaining amplifier and on the phase and power lock loops can be found
145 in [24]. A thermal sensor (Cernox 1070) and a resistive heater are embedded in the cavity post. The resonator temperature is stabilized using a LakeShore 336 temperature controller [25].

3.2. Base temperature requirement

150 The turnover temperature at which the resonator thermal sensitivity vanishes is specific to each crystal [26]. It is generally found between 5 K and 9 K for the high-quality crystals we use. To safely cool down the resonator with a sufficient margin for proper temperature stabilisation, the requirement on minimum achievable temperature has been set to 4.5 K. We demonstrated in
155 [13], that a cooling power of about 100 mW is required depending on the choice of materials and geometry of the suspending rods, copper braids and thermal shields.

3.3. Cryocooler choice and design constraints

The GM Sumitomo RDK-101 was chosen as cold source for the new prototype. The RDK-101 is a two-stage Gifford-McMahon Cryocooler, with a second-stage capacity of 0.16 W @ 4.2 K and operated with water cooled compressor consuming 2.4 kW. The fundamental frequency of its thermodynamical cycle is 1 Hz. The experiments presented here are part of a larger study for which we wish to compare in a future step several cryocoolers to cool down the same cryostat. Thus, the design of the support structures will have to involve adaptation parts to compensate for the different geometries between the cryocoolers we want to test. Ultimately, the CSOs we are studying are destined to become autonomous instruments that will have to be integrated into an existing infrastructure and sometimes operated in remote sites. Overall size and weight are then to be considered.

3.4. Mitigation of the cold-finger vibrations

The motion of the cold finger due to the deformation of the tubes linking it to the cold head is transferred to the resonator through the copper braids. At a comparable cooling power, this deformation is of the same order of magnitude for the two types of cryocooler. Tomaru [27] measured only twice as much displacement for a GM compared to a PT. The transferred displacement is attenuated by the ratio between the stiffness of the copper braids and that of the suspension rods. In [13] we showed how the tradeoff between the transfer of the cooling power and that of the vibrations was found for a PT by using specially designed V-shaped 3D-printed Mylar rods. These Mylar suspensions revealed to effectively mitigate the vibration transferred to the resonator in the vertical direction $O\vec{z}$. However, they transversal stiffness remains still poor due to the low value of the Mylar Young modulus. In this new prototype, we opted for V-shaped rods made with 6×5.7 mm^2 stainless steal tubes, offering higher transversal thickness.

3.5. Mitigation of the cold-head vibrations

The cold head motion is due to the action of the mechanical displacer for a GM or to the pressure impact for a PT. From Tomaru the corresponding acceleration is 100 times higher for a GM than for a PT. So here lies the main difficulty of using a GM. A solution is to clamp the cold-head on a very rigid frame independent of the cryostat. The connection between the two is made with a bellows. This solution proposed by Ikushima [28] is hardly compatible with our constraints of volume and weight. These require us to keep the ULISS-2G design where the cryostat vacuum chamber itself acts as a support structure. In this configuration, the cold head displacement exerts a force on the top flange of the vacuum chamber through the bellows. As the vacuum chamber rigidity is not infinite, its displacement is transferred to the resonator through the holding rods. In this case the ratio between the stiffness of the bellows and that of the vacuum chamber determines the degree of mechanical attenuation. We therefore sought to increase the rigidity of the cryostat vacuum chamber while maintaining a weight for the entire device not exceeding 80 kg. Many configurations were simulated and evaluated numerically. One of the optimisation criteria was to push any mechanical resonance of the empty chamber well beyond 100 Hz. The configuration we have finally chosen is represented in the figure 6.

The vacuum chamber is made in 316L SS. The wall thickness is 3 mm instead of 1.5 mm in the ULISS-2G initial design. Lateral reinforcements were welded on the outer wall: i) 20×20 mm SS square solid bars and ii) SS rings 10 mm thick. The first mechanical resonance of this structure, i.e. the one with the lowest frequency, is at about 350 Hz and corresponds to the flexion mode of the vacuum chamber for which the top flange is moved transversely. Finally, the cold-head supported by the bellows constitutes a mechanical resonator oscillating in the vertical direction. Its resonance frequency is $\sqrt{k/M}/2\pi \approx 20$ Hz, where M is the mass of the cold-head and k the axial stiffness of the bellows. To limit the amplitude of this resonance, four Sorbothane dampers [29] have been implemented under the cool head. The preloading applied on these dampers can be adjusted with screws. In the interior view (right on figure 5), note the

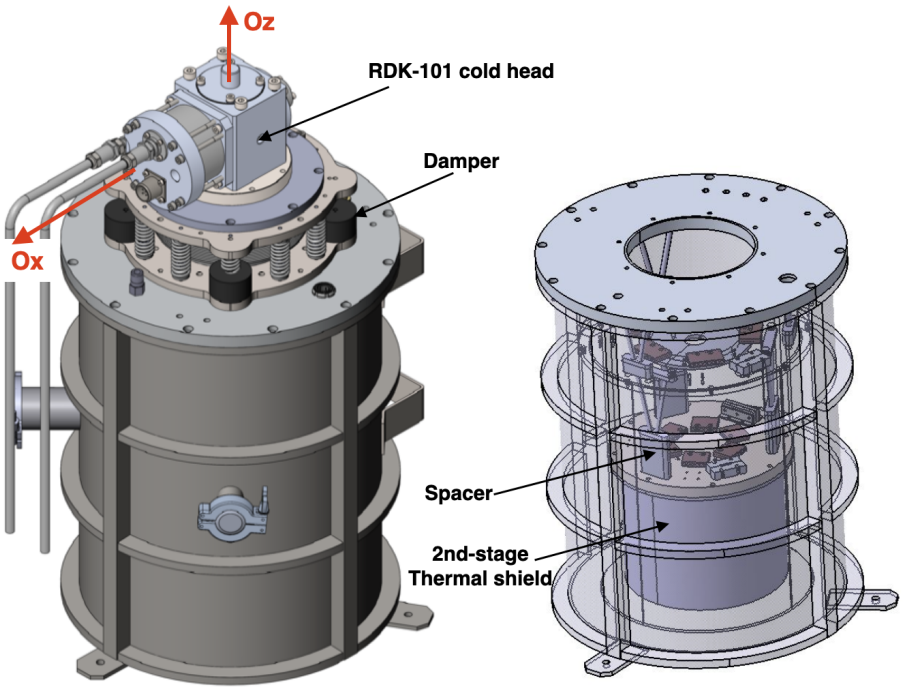

Figure 6: New CSO cryostat. Left: view from outside. Right: view of the interior.

adaptation parts (spacers) that extend the suspension bars. By lengthening the suspension we guarantee the geometric compatibility with different cold heads, at the cost of reducing the transverse stiffness of the suspension. From this point of view, the optimisation is not complete and better results are expected with a more adapted geometry.

3.6. Thermal budget

As the mechanical design is complete, we must verify that this cryostat is able to achieve the required minimum temperature, i.e., 4.5 K. We followed the same procedure described in [13]. The experimental parameters we used for this evaluation are given in the table 1.

The table 2 gives the expected temperature and radiative and conductive contributions to the thermal budget from both the 1^{st} and 2^{nd} stage of the

Table 1: Parameters used for the thermal budget evaluation. The emissivity values have been drawn from [31]

1^{st}**-stage**		geometry	emissivity
Emitting surface	vacuum SS chamber	$S_0 = 0.6$ m^2	$\epsilon_0 = 0.4$
Receiving surface	1^{st} shield (gold platted Cu)	$S_1 = 0.325$ m^2	$\epsilon_1 = 0.03$
Holding rods	$6 \times$ SS 6×5.7 mm tubes	$L_1 = 90$ mm	
Cu braids thermal resistance	$R_1 = 1$ K/W		
RF cables	$4\times$ BeCu UT-085	$L = 150$ mm	
2^{nd}**-stage**			
Emitting surface	1^{st} shield	$S_1 = 0.325$ m^2	$\epsilon_1 = 0.03$
Receiving surface	2^{nd} shield (gold platted Cu)	$S_2 = 0.155$ m^2	$\epsilon_2 = 0.02$
Holding rods	$6 \times$ SS 6×5.7 mm tubes	$L_2 = 90$ mm	
Cu braids thermal resistance	$R_2 = 7$ K/W		
RF cables	$4\times$ BeCu UT-085	$L = 190$ mm	

cryostat.

Table 2: Thermal budget. $P_{\rm rad}$: radiative contribution, $P_{\rm cables}$ and $P_{\rm sus}$: conductive contribution of the microwave cables and suspension rods respectively.

	T	$P_{\rm cables}$	$P_{\rm sus}$	$P_{\rm rad}$
1^{st}-stage	43.1 K	0.85 W	0.54 W	4.1 W
2^{nd}-stage	3.4 K	19.4 mW	19.7 mW	0.4 mW

The 1st stage receives 5.5 W heating power coming mainly from the radiation of the 300 K vacuum chamber. Its temperature stabilises at 43.1 K. The second stage at the resonator level stabilises at 3.4 K and receives 40 mW mostly due to the thermal conduction through the suspending rods and the microwave cables. We thus obtain a safety margin of about 1 K on the minimum achievable temperature. The previous analysis already used to validate the first ULISS-2G cryostat is considered reliable enough to undertake the construction of a prototype.

4. Acceleration measurements

The cryostat having been realized, preliminary acceleration measurements were carried out to validate the mechanical design and to consolidate the numerical simulations. Two seismic accelerometers (Bruel & Kjaer model 8344 [30]) were set in place of the resonator to measure the acceleration in the vertical $O\vec{z}$ and transverse $O\vec{x}$ directions (see figure 6). These measurements were performed when the cryocooler was started because the accelerometers are not calibrated below -50 °C. The figure 7 shows the measured acceleration PSD.

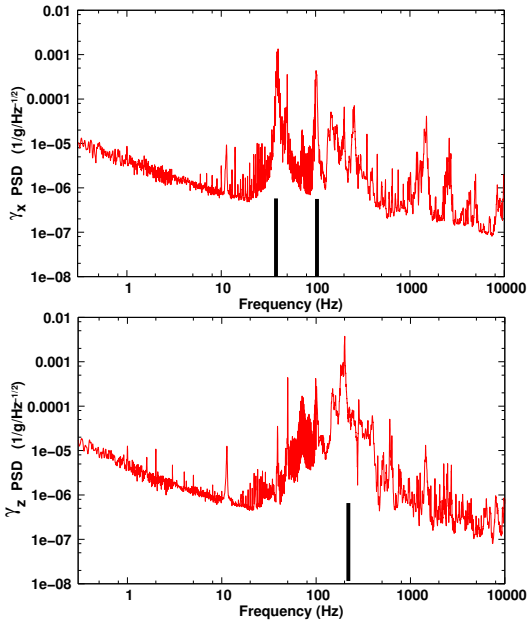

Figure 7: *Acceleration power spectral density along $O\vec{x}$ (above) and $O\vec{z}$ (down). The resolution bandwidth (RBW) is 12 mHz for 1 Hz $\leq f \leq$ 10 Hz. Bold bars: first mechanical resonances of the cryogenic assembly (see Fig. 8).*

4.1. Analysis of the measured acceleration PSD

For the two directions, the peaks corresponding to the cryocooler fundamental frequency (1 Hz) and its first harmonics barely come out of the noise floor. The table 3 summarizes the measured accelerations and associated displacements for $f_m = 1$ Hz and the first three harmonics.

Table 3: Measured rms accelerations and associated displacements.

f_m (Hz)	γ_x (μg)	x (nm)	γ_z (μg)	z (nm)
1	0.8	200	1.3	330
2	–	–	1.1	70
3	–	–	0.5	10
4	–	–	0.3	4

The line at 10 Hz comes from the pumping system connected to the vacuum chamber to maintain a residual pressure below 1×10^{-4} mb during the measurement. In nominal CSO operation, this pumping system is stopped when the thermal steady state is reached. The cryopumping is sufficient to maintain the pressure below 1×10^{-7} mb when the 2^{nd} stage is stabilised around 6 K. Above 10 Hz, the mechanical resonances of the cryogenic assembly amplify the impact of the cryocooler vibrations populating the spectra with mainly spurious lines. We identified these mechanical resonances by simulating the overall assembly, i.e., vacuum enclosure + cryogenic assembly, using Comsol Multiphysique software. The first resonance modes (those with the lowest frequency), that have significative participation factor for each direction are represented in the figure 7. The modal participation factor is a measure of how strongly a given mode contributes to the response of the structure when subjected to force/displacement excitation in a specific direction.

The figure 8 (left) represents the first mechanical resonance giving a noticeable displacement in the $O\vec{x}$ direction. This pendulum mode makes the two stages oscillating in phase at 38 Hz. In the same direction, the second resonance mode (not represented in the figure) is the pendulum mode with the two stages oscillating out of phase at 101 Hz. The first mechanical resonance for the $O\vec{z}$ direction is represented in the figure 8 (right). It is characterised by a deformation (bulging) of the vacuum enclosure flanges and a frequency of 204 Hz. Pushing these resonances at higher frequency and/or increase they

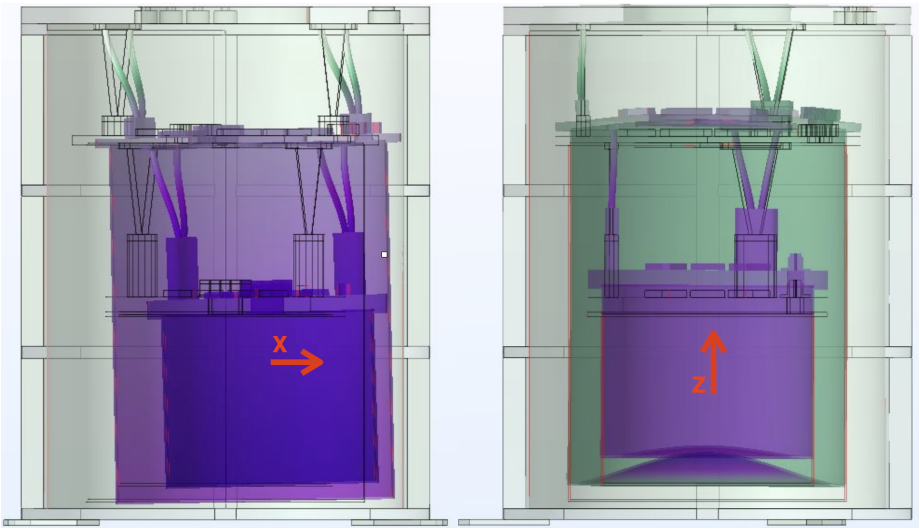

Figure 8: *First mechanical resonance modes of the whole structure. The effect of the displacement shown in the pictures is amplified to make it more evident.*

dissipation is difficult without increasing the thermal load of the two cryocooler stages. However, as $\sigma_{y_{\min}}(\tau) \propto 1/f_m$ their current resonance frequency are high enough to not affect the CSO 's short-term frequency stability above $\tau = 1$ s, which is the main performance objective to reach.

4.2. Expected phase noise degradation

To give an order of magnitude of the phase noise degradation due to the acceleration, we only take into account the contribution along the vertical $(O\vec{z})$ direction. Indeed, it is in this direction that the sensitivity of the resonator and its acceleration are the highest. Injecting in the equation 2, the values $\Gamma_z = 1 \times 10^{-9}/$ g and $\gamma_z = 1.3 \times 10^{-6}$ g, the expected power contained in the 1 Hz line is:

$$S_{\varphi_{\text{expect.}}}(1 \text{ Hz}) = -97.7 \text{ dBrad}^2 \tag{5}$$

This expected value combines the measurement of the resonator sensitivity and that the acceleration. It will compared later (see section 5) to oscillator phase noise spectrum.

4.3. About room temperature measurements

We are aware that measurements made at room temperature may differ from the actual behavior at low temperature. Indeed, the mechanical properties of the materials vary between 300 K and 4 K. Nevertheless, this variation is expected to be small for stainless steel, copper [32] and sapphire [33], which are the main constituents of the cryogenic system. In a first step, we thus assume that the previous measurements give orders of magnitude that stay representative at low temperature. This assumption has been validated *a posteriori* by the oscillator charaterization described in the following section.

5. Oscillator characterisation

After the preliminary characterization step described in the previous section, the resonator is mounted in the cryostat described in the section 3 with all the components necessary for the oscillator operation and the cryocooler compressor is switched on.

5.1. Achieved temperatures

The figure 9 shows the evolution of the temperature of the two stages.

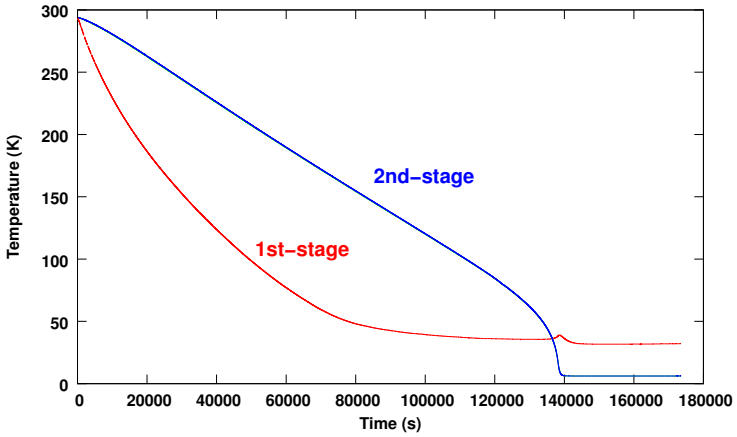

Figure 9: 1^{st} *and* 2^{nd} *stage temperature evolutions during cool-down.*

At steady state, the temperatures of each stage are: $T_1 = 31$ K and $T_2 = 4.2$ K. These values differ from those expected (see section 3.6). This may indicate that the current cooling power available at each stage differs from what we expected from the manufacturer's data sheet. Another cause of uncertainty lies in the values of emissivities attributed to the different surfaces in our thermal budget. Indeed, the emissivity of a surface depends on many parameters: roughness, oxidation, cleanliness... which are difficult to control. However, T_2 is compatible with our need and comparable to the lowest temperature obtained with the PT403. We note the cool down time necessary to achieve the steady state is $\sim$ 39 h. That is more than two times than that obtained with the PT403. This is not an issue for our application as the CSO is expected to run continuously for months or even for years. The sapphire crystal implemented in this cryostat is characterised by turnover temperature of 6.3 K. During the implementation of this new cryostat, it underwent multiple dismounting and cooling downs. We observed a loss in its unloaded quality factor starting from one billion to 7×10^8, certainly due to the deposition of contaminants on the resonator surface. Moreover, we did not refine its input and output couplings. They are characterised by the coupling coefficients [34]: $\beta_1 = 1.1$ and $\beta_2 = 0.02$, respectively. As a reminder, the optimum configuration for the Pound servo loop is a resonator critically coupled at its input, which means: $1 - \beta_1 + \beta_2 = 0$. Despite these non-optimal conditions, the resonator parameters are still compatible with the ULISS-2G specification: $\sigma_y(\tau) < 3 \times 10^{-15}$ for 1 s $\leq \tau \leq 10^4$ s.

5.2. Frequency stability measurement set-up

We compared the new prototype to one of the reference CSOs of our laboratory [35]. We use the classical beatnote method [16] with a measurement setup schematized in the figure 10.

The reference source is a 1$^{\text{st}}$ generation CSO equipped with a 6 kW PT405 cryocooler [36]. It is characterised by fractional frequency stability better than 1×10^{-15} for 1 s $\leq \tau \leq 10,000$ s. The two CSO's signals are mixed to get a beatnote at 7.4 MHz. The phase noise and Allan deviation data were directly

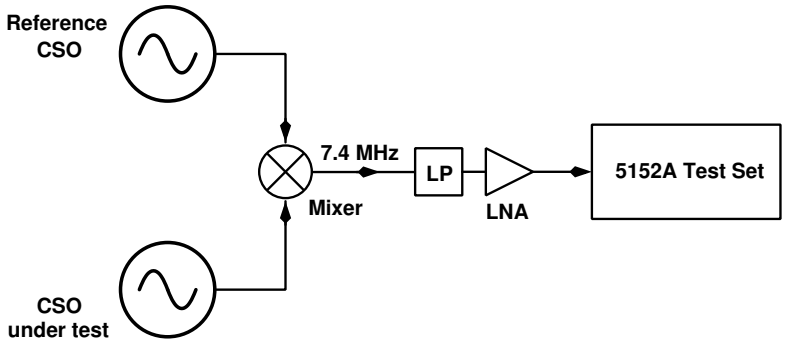

Figure 10: *Frequency stability measurement set up. (Mixer: Frequency mixer, LP: Low pass filter, LNA: low noise amplifier)*

collected with a Symmetricom 5125A Test Set [37].

5.3. Phase Noise Power Spectral Density

The phase noise Power Spectral Density (PSD) is shown in the figure 11.

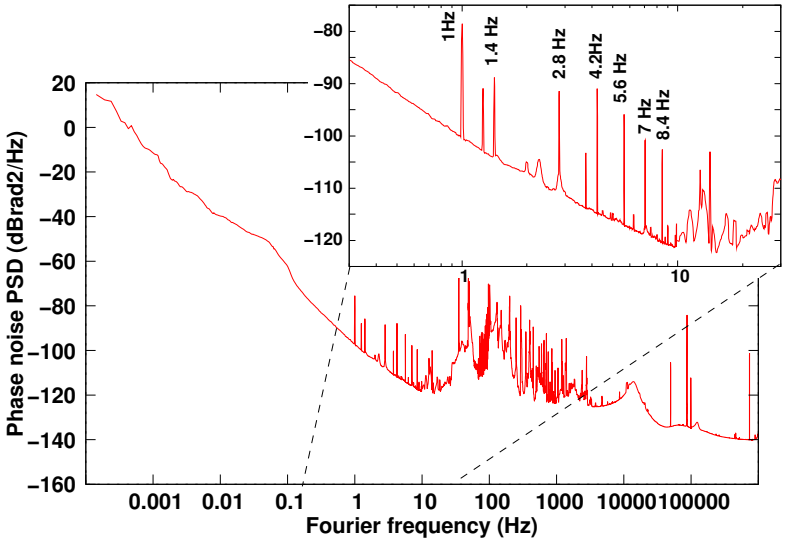

Figure 11: *Phase noise PSD obtained by beating the two CSOs. The measurement resolution bandwidth is* 12 *mHz @* 1 *Hz.*

The obtained PSD is similar to what it is generally observed by beating 2 CSOs [23, 38]. The spread bump near 0.1 Hz results from residual temperature

fluctuations. We will see later its signature on the Allan deviation curve. The one near 10 kHz is signature of the Pound lock loop bandwidth. The numerous spurious between 1 Hz and 1 kHz are the result of the mechanical vibrations originating from the two CSOs. The insert in the figure 9 serves to distinguish the contribution of each cryogenic oscillator.

The 1 Hz line comes from the CSO under test equipped with the GM RDK-101 cryocooler, that at 1.4 Hz from the reference oscillator. It is worth noting that the other strong spurious lines visible on the spectrum are all harmonics of the fundamental frequency of the PT-405, and thus are due to the reference oscillator. Taking into account of the 12.5 mHz resolution bandwidth of the Symmetricom 5125A, the power in the 1 Hz spurious line is:

$$S_\varphi(1 \text{ Hz}) = -95 \text{ dBrad}^2 \tag{6}$$

The difference with the expected value is less than 3 dB (see equation 5). This may be due to the contribution of the transverse acceleration neglected in the calculation of the expected phase noise degradation.

Always assuming that the acceleration is along $(O\vec{z})$ and $\Gamma_z = 1 \times 10^{-9}/\text{g}$, we calculated the acceleration and the displacement at the fundamental frequency of the CSO under test. We found $\gamma_z \sim 1.8$ μg and $z \sim 450$ nm. For comparison, the line at 1.4 Hz coming from the reference oscillator we have: $S_\varphi(1.4 \text{ Hz}) = -105 \text{ dBrad}^2$, corresponding to a rms acceleration of 0.8 μg and a displacement of 100 nm.

We conclude that the phase noise PSD obtained with the reinforced cryostat equipped with the GM is not really degraded relative to that obtained with 1st generation CSO.

5.4. Allan Deviation

The previous conclusion in confirmed by the ADEV represented in the figure 12.

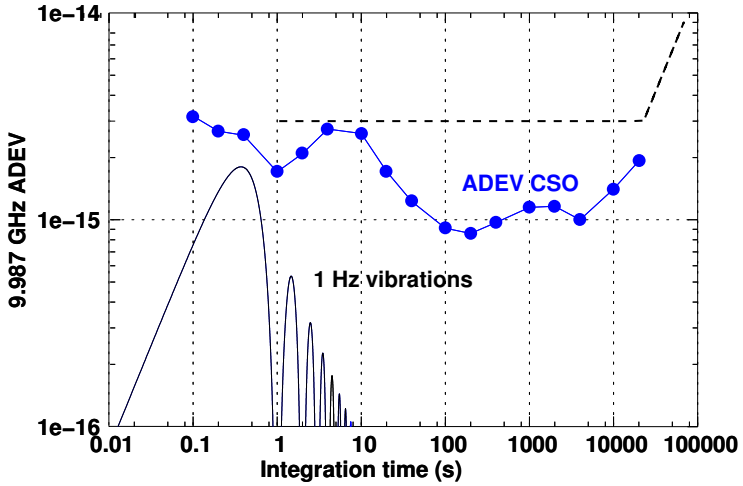

Figure 12: *Frequency stability measurement results compared to the contribution of the 1 Hz mechanical vibrations.*

—●— : Allan Deviation obtained by beating the two CSOs.

— : $\sigma_{y_{min}}(\tau)$ with $\Gamma = 1 \times 10^{-9}/g$, $\gamma_z = 1.8$ μg and $f_m = 1$ Hz.

- - : ULISS-2G specification.

The measured ADEV is compatible with the ULISS-2G specification, demonstrating that a GM cryocooler can be a valuable alternative to the PT cryocooler. The curve in black in the figure 10 represents $\sigma_{y_{\rm min}}(\tau)$ calculated with the $\Gamma = 1 \times 10^{-9}$/g and $\gamma_z = 1.8$ μg. The 1 Hz vibration generated by the cryocooler does not interfere with frequency stability for $\tau \geq 1$ s. The bump in the ADEV near 10 s result from an imperfection of the resonator temperature control. In [1, 23], we have shown how unexpected time lag in the thermal system and the relative slowness of the digital temperature control induce small and slow temperature modulation in the resonator. This modulation originates bumps in the phase noise PSD and ADEV curves. Better short term stability are obtained with resonator operating at a lower temperature.

6. Summary

In this paper we demonstrate for the first time the achievement of a state-of-the-art fractional frequency stability with a CSO operated with a low power Gifford-McMahon cryocooler. This cryogenic microwave oscillator achieves a fractional frequency stability better than 3×10^{-15} for integration time up to $10,000$ s. Simple passive solutions have been implemented to efficiently mitigate the transfer of the mechanical cryocooler vibrations to the cryogenic resonator. Our design is based on a stiffened vacuum chamber that supports the cryogenic assembly. The experimental load is suspended from this frame by rigid bars, the cooling power being transferred by flexible copper braids. The optimization of the different subsystems was realized using numerical simulations. The rms displacements of the experimental load measured at room temperature and at the fundamental frequency of the GM are 330 nm in the axial direction and 200 nm in the transverse direction. The measurement of the CSO phase noise demonstrates that the order of magnitude of these displacements remains unchanged at low temperature.

References

[1] C. Fluhr, B. Dubois, G. L. Tetu, V. Soumann, J. Paris, E. Rubiola, V. Giordano, Reliability and reproducibility of the cryogenic sapphire oscillator technology, IEEE Transactions on Instrumentation and Measurement 72 (2023) 1–8. doi:10.1109/TIM.2023.3277940.

[2] C. Fluhr, B. Dubois, C. E. Calosso, F. Vernotte, E. Rubiola, V. Giordano, A cryogenic sapphire resonator oscillator with 10^{-16} mid-term fractional frequency stability, Applied Physics Letters 123 (4) (2023) 044107. doi:10.1063/5.0153711.

[3] G. Santarelli, P. Laurent, P. Lemonde, A. Clairon, A. G. Mann, S. Chang, A. N. Luiten, C. Salomon, Quantum projection noise in an atomic fountain:

A high stability cesium frequency standard, Physical Review Letters 82 (23) (Jun. 1999).

[4] M. Abgrall, J. Guéna, M. Lours, G. Santarelli, M. Tobar, S. Bize, S. Grop, B. Dubois, C. Fluhr, V. Giordano, High-stability comparison of atomic fountains using two different cryogenic oscillators, IEEE Transactions on Ultrasonics, Ferroelectrics, and Frequency Control 63 (8) (2016) 1198–1203.

[5] R. T. Wang, M. Calhoun, A. Kirk, W. Diener, G. Dick, R. Tjoelker, A high performance frequency standard and distribution system for cassini ka-band experiment, in: Proceedings of the 2005 IEEE International Frequency Control Symposium and Exposition, 2005., IEEE, 2005, pp. 919–924.

[6] M. Rioja, R. Dodson, Y. Asaki, J. Hartnett, S. Tingay, The impact of frequency standards on coherence in VLBI at the highest frequencies, The Astronomical Journal 144 (4) (2012) 121.
URL http://stacks.iop.org/1538-3881/144/i=4/a=121

[7] B. Alachkar, A. Wilkinson, K. Grainge, Frequency reference stability and coherence loss in radio astronomy interferometers application to the SKA, Journal of Astronomical Instrumentation 7 (01) (2018) 1850001.

[8] P. L. Stanwix, M. E. Tobar, P. Wolf, M. Susli, C. R. Locke, E. N. Ivanov, J. Winterflood, F. van Kann, Test of lorentz invariance in electrodynamics using rotating cryogenic sapphire microwave oscillators, Phys. Rev. Lett. 95 (4) (2005) 040404. doi:10.1103/PhysRevLett.95.040404.

[9] W. M. Campbell, B. T. McAllister, M. Goryachev, E. N. Ivanov, M. E. Tobar, Searching for scalar dark matter via coupling to fundamental constants with photonic, atomic, and mechanical oscillators, Physical Review Letters 126 (7) (2021) 071301.

[10] H. Ball, W. D. Oliver, M. J. Biercuk, The role of master clock stability in

quantum information processing, npj Quantum Information 2 (1) (2016) 1–8.

[11] Ting Rei Tan, T. Navickas, C. Valahu, J. Jee, A. Rao, M. Millican, M. Biercuk, Improving a trapped-ion quantum computer with a Cryogenic Sapphire Oscillator, in: Proceedings of the 2023 joint meeting IEEE International Frequency Control Symposium and 17th European Frequency and Time Forum, Toyama (J), 2023, p. to be published.

[12] J.-M. Le Floch, Y. Fan, G. Humbert, Q. Shan, D. Férachou, R. Bara-Maillet, M. Aubourg, J. G. Hartnett, V. Madrangeas, D. Cros, J.-M. Blondy, J. Krupka, M. E. Tobar, Invited Article: Dielectric material characterization techniques and designs of high-Q resonators for applications from micro to millimeter-waves frequencies applicable at room and cryogenic temperatures, Review of Scientific Instruments 85 (3) (2014) 031301. doi:10.1063/1.4867461.

[13] C. Fluhr, B. Dubois, S. Grop, J. Paris, G. Le Tetû, V. Giordano, A low power cryocooled autonomous ultra-stable oscillator, Cryogenics 80 (2016) 164–173.

[14] http://www.cryomech.com/ (Accessed Aug. 17, 2023).

[15] R. L. Filler, The acceleration sensitivity of quartz crystal oscillators: A review, IEEE Transactions on Ultrasonics, Ferroelectrics, and Frequency Control 35 (3) (1988) 297–305.

[16] E. Rubiola, F. Vernotte, The Companion of Enrico's Chart for Phase Noise and Two-Sample Variances, IEEE Transactions on Microwave Theory and Techniques (2023) 1–30, doi:10.1109/TMTT.2023.3238267.

[17] A. N. Luiten, Sapphire secondary frequency standards., Ph.D. thesis, Universitty of Western Australia, Perth, W.A. (1995).

[18] M. Oxborrow, K. Benmessai, S. Grop, N. Bazin, P. Bourgeois, Y. Kersalé, V. Giordano, g-sensitivity of a cryogenic sapphire resonator, in: Proc. 22nd

European Frequency and Time Forum, Toulouse, France, 2008, pp. FPE–062.

[19] P. Stockwell, C. McNeilage, M. Mossammaparast, D. Green, J. Searls, 3-Axis vibration performance of a compact sapphire microwave oscillator, in: Proc. of the 2001 IEEE International Frequency Control Symposium., Seattle, Wa, US, 2001, pp. 695–698.

[20] R. Pound, Electronic frequency stabilization of microwave oscillators, Review of Scientific Instruments 17 (11) (1946) 490–505.

[21] E. Black, An introduction to Pound-Drever-Hall laser frequency stabilization, Am. J. Phys 1 (2001) 79–87.

[22] https://www.rohde-schwarz.com (Accessed Aug. 17, 2023).

[23] C. Fluhr, S. Grop, B. Dubois, Y. Kersalé, E. Rubiola, V. Giordano, Characterization of the individual short-term frequency stability of cryogenic sapphire oscillators at the 10^{-16} level, IEEE Transactions on Ultrasonics, Ferroelectrics and Frequency Control 63 (6) (2016) 915–921.

[24] S. Grop, P. Y. Bourgeois, N. Bazin, Y. Kersalé, E. Rubiola, C. Langham, M. Oxborrow, D. Clapton, S. Walker, J. De Vicente, V. Giordano, ELISA: A cryocooled 10 GHz oscillator with 10^{-15} frequency stability, Review of Scientific Instruments 81 (2) (2010) 025102. doi:http://dx.doi.org/10.1063/1.3290631.

[25] Lake Shore Cryotronics Inc., 575 McCorkle Blvd, Westerville, OH (US), User's Manual, Model 336 Temperature controler.

[26] V. Giordano, C. Fluhr, S. Grop, B. Dubois, Tests of sapphire crystals manufactured with different growth processes for ultra-stable microwave oscillators, IEEE Transactions on Microwave Theory and Techniques 64 (1) (2016) 78–85.

[27] T. Tomaru, T. Suzuki, T. Haruyama, T. Shintomi, A. Yamamoto, T. Koyama, R. Li, Vibration analysis of cryocoolers, Cryogenics 44 (5) (2004) 309–317.

[28] Y. Ikushima, R. Li, T. Tomaru, N. Sato, T. Suzuki, T. Haruyama, T. Shintomi, A. Yamamoto, Ultra-low-vibration pulse-tube cryocooler system–cooling capacity and vibration, Cryogenics 48 (9) (2008) 406–412.

[29] https://www.thorlabs.com (Accessed Aug. 17, 2023).

[30] https://www.bksv.com/fr/transducers/vibration/accelerometers/ (Accessed Aug. 17, 2023).

[31] J. Frolec, T. Králík, V. Musilová, P. Hanzelka, A. Srnka, J. Jelínek, A database of metallic materials emissivities and absorptivities for cryogenics, Cryogenics 97 (2019) 85–99. doi:https://doi.org/10.1016/j.cryogenics.2018.12.003.

[32] J. Ekin, Experimental techniques for low-temperature measurements: cryostat design, material properties and superconductor critical-current testing, Oxford university press, 2006.

[33] W. E. Tefft, Elastic constants of synthetic single crystal corundum, Journal of Research of the National Bureau of Standards. Section A, Physics and Chemistry 70 (4) (1966) 277.

[34] R. E. Collin, Foundations for microwave engineering, John Wiley & Sons, New York, 2007, ISBN 0-7803-6031-1.

[35] https://www.femto-engineering.fr/en/equipement/oscillator-instability-measurement-platform/ (Accessed June. 15, 2023).

[36] V. Giordano, S. Grop, C. Fluhr, B. Dubois, Y. Kersalé, E. Rubiola, The autonomous cryocooled sapphire oscillator: A reference for frequency stability and phase noise measurements, Journal of Physics: Conference Series 723 (1) (2016) 012030.

[37] https://www.microsemi.com/product-directory/phase-noise-and-allen-deviation-testers/4129-5125a. (Accessed Aug. 17, 2023).

[38] J. G. Hartnett, N. R. Nand, C. Lu, Ultra-low-phase-noise cryocooled microwave dielectric-sapphire-resonator oscillators, Applied Physics Letters 100 (18) (2012) 183501(1–4).